Journal of Magnetic Resonance **143,** 184–196 (2000)
doi:10.1006/jmre.1999.1979, available online at http://www.idealibrary.com on IDEAL®

Evaluation of Cross-Correlation Effects and Measurement of One-Bond Couplings in Proteins with Short Transverse Relaxation Times

Georg Kontaxis, G. Marius Clore, and Ad Bax

Laboratory of Chemical Physics, National Institute of Diabetes and Digestive and Kidney Diseases, National Institutes of Health, Bethesda, Maryland 20892-0520

Received September 1, 1999; revised October 15, 1999

Various strategies are described and compared for measurement of one-bond J_{NH} and $J_{NC'}$ splittings in larger proteins. In order to evaluate the inherent resolution obtainable in the various experiments, relaxation rates of ^{15}N–$^{1}H^{N}$ coupled and heteronuclear decoupled resonances were measured at 600- and 800-MHz field strengths for both perdeuterated and protonated proteins. A comparison of decay rates for the two ^{15}N–{H^{N}} doublet components shows average ratios of 4.8 and 3.5 at 800- and 600-MHz ^{1}H frequency, respectively, in the perdeuterated proteins. For the protonated proteins these ratios are 3.2 (800 MHz) and 2.4 (600 MHz). Relative to the regular HSQC experiment, the enhancement in TROSY ^{15}N resolution is 2.6 (perdeuterated; 800 MHz), 2.0 (perdeuterated; 600 MHz), 2.1 (protonated; 800 MHz), and 1.7 (protonated; 600 MHz). For the ^{1}H dimension, the upfield $^{1}H^{N}$–{^{15}N} component on average relaxes slower than the downfield $^{1}H^{N}$–{^{15}N} component by a factor of 1.8 (perdeuterated; 800 MHz) and 1.6 (perdeuterated; 600 MHz). The poor resolution for the upfield ^{15}N–{^{1}H} doublet component in slowly tumbling proteins makes it advantageous to derive the J_{NH} splitting from the difference in frequency between the narrow downfield ^{15}N doublet component and either the ^{1}H-decoupled ^{15}N resonance or the peak position in an experiment which *J*-scales the frequency of the upfield doublet component but maintains some of the advantages of the TROSY experiment.

1. INTRODUCTION

A variety of different approaches have been proposed to extend solution NMR to larger proteins (*1–11*). A combination of heteronuclear triple resonance NMR with perdeuteration (*5–10*) is particularly powerful in this respect and makes it possible to obtain backbone resonance assignments for systems of up to 50 kDa (*11–14*). Recent experiments which take advantage of relaxation interference can extend this range even further (*9, 15–18*). However, the lower proton spin density in such perdeuterated proteins also results in a dramatic drop in the number of observable NOE interactions. Although this can be mitigated to some extent by reintroducing protonated methyl groups in such proteins (*7*), which typically provide invaluable long-range NOE constraints, this NOE information remains too limited for defining the molecular structure at high accuracy (*19*).

Next to NOE constraints, residual one-bond dipolar couplings, which can be measured in weakly oriented macromolecules, also hold considerable potential for increasing the accuracy of molecular structures (*20–24*). With the introduction of a dilute nematic liquid crystal medium consisting of oriented phospholipid particles commonly known as bicelles (*25, 26*), which can be used to induce alignment of a protein in the aqueous phase, measurement of dipolar couplings has become much easier (*27–29*). Other media have also been proposed, which widen the area of applicability even further (*30–34*).

For many proteins the ^{15}N–^{1}H HSQC spectra are reasonably well resolved. Because the ratio of the heteronuclear ^{15}N–^{1}H dipolar coupling over the ^{15}N linewidth is favorable, one-bond $^{1}D_{NH}$ couplings are usually the easiest to measure. However, when shifting to larger proteins the effect of interference between the ^{15}N chemical shift anisotropy and one-bond ^{15}N–^{1}H dipolar coupling relaxation mechanisms results in very different linewidths of the two ^{15}N–{^{1}H} doublet components (*35, 36*). Thus, although the downfield doublet component remains relatively sharp, even for larger proteins, the upfield component is typically much broader, depending on the strength of the magnetic field and the magnitude and orientation of the CSA tensor of the ^{15}N in question. This differential relaxation mechanism is used to great advantage in the TROSY-based experiments, which selectively detect only the narrowest of the heteronuclear multiplet components (*9, 16, 37*) and greatly increase spectral resolution relative to their conventional, non-TROSY analogs. However, the accuracy at which $^{1}D_{NH}$ can be measured from a F_1-coupled ^{15}N–^{1}H HSQC spectrum is primarily determined by the accuracy at which the frequency of the broad upfield ^{15}N–^{1}H doublet component can be determined. For larger proteins, where the linewidth of this doublet component can be forbiddingly large, this can adversely affect spectral resolution and sensitivity and thereby the accuracy at which the one-bond ^{1}H–^{15}N dipolar couplings can be measured. Here, we show that it can be advantageous to obtain the dipolar coupling from the difference in ^{15}N frequency in a TROSY spectrum and in a de-

1090-7807/00

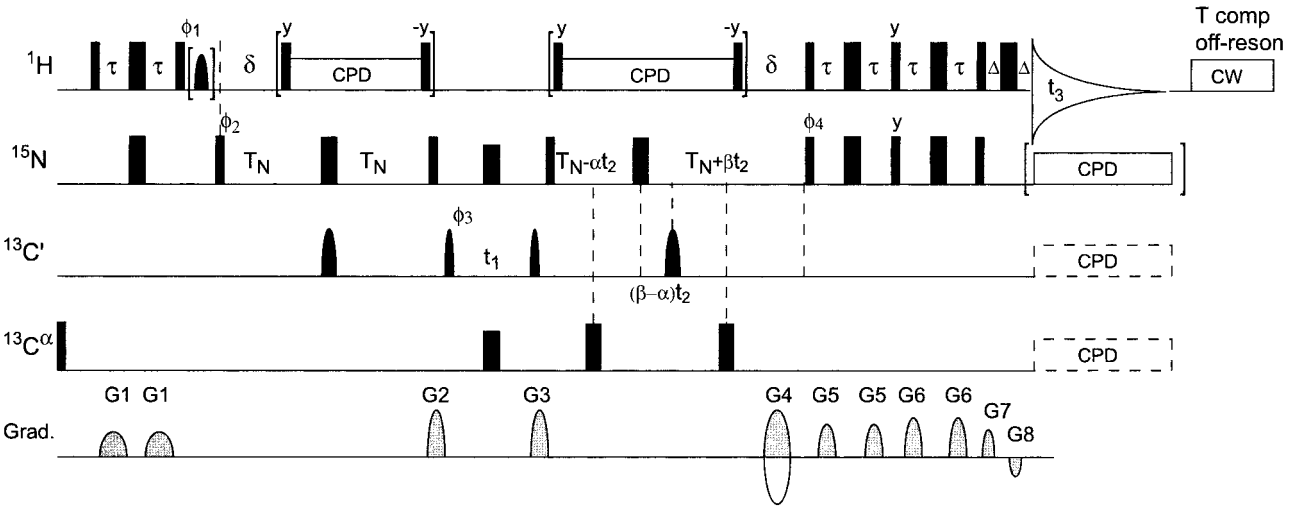

FIG. 1. Pulse schemes for the cpd-HNCO and TROSY-HNCO experiments. Narrow and wide pulses correspond to 90° and 180° flip angles, respectively. Pulse phases are *x*, unless otherwise indicated. The experiment can be conducted in the $^1H^N$–^{15}N cpd-decoupled mode (with the ^1H pulses between square brackets included) and corresponding closely to the pulse scheme of Kay *et al.* (*40*) or in the TROSY-HNCO manner (by deleting the ^1H pulses and ^{15}N decoupling between square brackets), yielding the scheme of Yang and Kay (*18*). Temperature compensation is obtained by ^1H irradiation off-resonance by 200 kHz at the end of each transient, such that the average amount of $^1H^N$ power per unit of time remains constant during the cpd-HNCO experiment, and to ensure that in the TROSY-HNCO the average ^1H RF power is the same as in the cpd-HNCO. Heating resulting from ^{15}N decoupling was found to be negligible in our experiments, but could be compensated for in a similar manner, if necessary. If measurement of the ^{15}N–$^{13}C'$ and $^1H^N$–$^{13}C'$ *J* splittings is desirable, the shaped $^{13}C'$ 180° pulse, applied during t_2 evolution, must be omitted. Note that accurate measurement of this splitting typically requires a t_{2max} value greater than ca. 100 ms, where t_{2max} is the length of the t_2 acquisition time. Both schemes include water-flip-back, either by active water-flip-back pulses (cpd-HNCO) or by radiation damping (TROSY-HNCO). Delay durations: $\tau = 2.6$ ms; $\delta = 5.3$ ms; $\Delta = 250$ μs; $T_N = 16.8$ ms. The ^{15}N t_2 evolution period is of the semi-constant-time type (*46*), and the parameters α and β are chosen such that $\alpha = T_N/t_{2max}$ and $\alpha+\beta = 1$. Phase cycling: $\phi_1 = y$ (for Bruker spectrometers); $\phi_2 = 2x,2(-x)$; $\phi_3 = x,-x$; receiver $= x,2(-x),x$. Quadrature detection in the t_1 dimension is obtained with the States–TPPI phase incrementation of ϕ_3 and in the t_2 dimension with the Rance–Kay method, altering the polarity of gradient G4 and inverting ϕ_4 (*44*). All gradients are sine-bell shaped with peak amplitudes of 30 G/Cm, and durations of G1 = 1.1 ms; G2 = 0.7 ms; G3 = 1.3 ms; G4 = 2.7 ms; G5 = 1.0 ms; G6 = 1.0 ms; G7 = 0.2 ms; G8 = 0.075 ms. Although not used in the experiments described here, decoupling of the $^{13}C'$ and $^{13}C^\alpha$ resonances during ^1H data acquisition is recommended (*58*), particularly in the liquid crystalline phase where these $^1H^N$–$^{13}C'$ couplings can be rather large.

coupled HSQC spectrum or from a 3D TROSY-HNCO and a novel *J*-scaled TROSY-HNCO spectrum.

EXPERIMENTAL

Samples and Hardware Used

The methods for measurement of ^{15}N–^1H couplings were tested for seven different samples: (1) 1 mM $^{15}N/^{13}C$-labeled ubiquitin (76 residues, 8.6 kD), pH 6.5, 10 mM phosphate buffer; (2) 1.5 mM $^{15}N/^{13}C/^2H$-labeled ubiquitin, pH 6.5, 10 mM phosphate buffer; (3) 0.5 mM ^{15}N-labeled ubiquitin, pH 6.5, 10 mM phosphate buffer, in a 5% w/v bicelle medium, with [DMPC]:[DHPC]:[CTAB] = 30:10:1; (4) 1.5 mM of ^{15}N-labeled N-terminal domain of Enzyme I (EIN, 259 residues, 30 kDa), 40 mM phosphate buffer, pH 7.5; (5) 0.8 mM of $^{15}N/^{13}C/^2H$-labeled EIN, 40 mM phosphate buffer, pH 7.5; (6) as (5), but also including 25 mg/ml bacteriophage *fd;* (7) 0.7 mM of a ^{15}N-Tyr-labeled Fab fragment of the TE33 antibody, raised against cholera toxin and kindly provided by Prof. J. Anglister. All samples were dissolved in 93% H_2O, 7% D_2O, in 270-μl thin-wall Shigemi microcells. The *fd*-containing EIN sample was 2 years old and showed signs of substantial proteolysis of the C-terminal flexible tail, resulting in extensive resonance overlap in the region near 8 ppm ^1H frequency, but with well-resolved resonances corresponding to peak positions in fresh EIN samples outside this region.

Experiments were carried out on Bruker DMX600, DMX750, and DRX800 spectrometers, all equipped with triple-resonance, three-axis pulsed field gradient probeheads. All measurements on EIN were carried out at 40°C, experiments on the Fab fragment at 37°C, and measurements on ubiquitin at 7°C, except for ubiquitin measurements in the bicelle medium which were carried out at 35°C. All spectra were processed and analyzed using the software package NMRPipe (*38*).

Pulse Sequences

In order to maximize sensitivity, all pulse schemes for measurement of *J* splittings included water-flip-back (*39*). Pulse schemes in which composite-pulse decoupling was used had this ^1H decoupling sequence bracketed by two 90° pulses (e.g., Fig. 1), in order to cause spin locking of the ^1H_2O magnetization instead of dephasing and saturation of the water magnetization (*40*). Schemes used for measurement of transverse relaxation rates did not include the water-flip-back fea-

ture because the efficiency of water-flip-back depends somewhat on the duration of the (variable) transverse relaxation delays and thereby could alter the apparent decay rate. Instead, longitudinal magnetization of both protein and water is effectively zero at the start of the FID, i.e., all ^{1}H magnetization recovers from the same saturated state for all durations of the relaxation delay.

Temperature Compensation

As the aim of the experiments is to extract the *J* splitting from the difference in peak position in two separate experiments, it is essential that the sample conditions are as similar as possible. Even when experiments are recorded in an interleaved or back-to-back manner, small differences in sample temperature can result from differences in the average radio-frequency power applied to the sample in the two experiments. The degree of sample heating increases dramatically with frequency, and ^{1}H decoupling in particular can significantly raise the sample temperature, even when using small duty cycles (<10%) and low power (~1 W). An easy way to avoid a difference in temperature relies on the introduction of dummy, off-resonance ^{1}H irradiation in the experiment which has the least amount of power dissipation, such that the average irradiation power becomes the same for both experiments (*41*). Such temperature compensation procedures were used for all experiments described here. Temperature compensation typically was accomplished by irradiating with an 8-kHz continuous wave ^{1}H RF field, 200 kHz downfield from the spectral region of interest.

Measurement of ^{15}N Decay Rates

Effective ^{15}N transverse magnetization decay constants were measured using both one-dimensional (all samples) and two-dimensional methods (ubiquitin). The upfield and downfield ^{15}N doublet components decay constants were measured in separate TROSY experiments, using phase cycling to select either the downfield or the upfield doublet component (*42, 43*), selecting the upfield ^{1}H doublet component during the detection period. A ^{15}N 180° pulse was added at the midpoint of the period which normally serves as the ^{15}N evolution period. Similarly, for the cpd-HSQC experiment, a 180° pulse was used at the midpoint of the ^{15}N evolution period, and 180° ^{1}H/^{15}N pulses during the $1/(2J_{NH})$ periods bracketing the decoupling sequence were omitted. The reverse INEPT contained a WATERGATE water suppression element (*44*) instead of Rance–Kay coherence selection (*45*). For the regular HSQC, also containing a WATERGATE-type reverse INEPT transfer, a ^{15}N 180° pulse was used at the midpoint of the regular evolution period, and two 180° ^{1}H pulses were inserted at time points corresponding to one quarter and three quarters of the evolution period, ensuring that a ^{15}N spin is coupled for equal amounts of time to a proton in the $|\alpha>$ and $|\beta>$ spin states. Relaxation times were derived from the decay rates of resolved resonances downfield of 8.5 ppm.

Transverse relaxation rates for the up- and downfield ^{15}N doublet components in ^{2}H/^{13}C/^{15}N ubiquitin were also measured using a two-dimensional sequence, with a Δ-180°(^{15}N)-Δ period preceding the regular evolution period in the TROSY (or anti-TROSY) experiment. For each type of measurement (1D, 2D, TROSY, HSQC) transverse decay periods were selected on the basis of preliminary measurement, so that they covered a range between zero and two times the estimated average decay times.

Measurement of $^1H^N$ Decay Rates

Transverse relaxation rates for the up- and downfield ^{1}H^N doublet components in ^{2}H/^{13}C/^{15}N ubiquitin were measured using a slightly modified HSQC experiment. A 90° ^{15}N purge pulse is added at the point where ^{15}N decoupling and ^{1}H^N data acquisition is normally started and, after this purge pulse, a WATERGATE spin-echo sequence (*44*), with a range of different durations for the de- and rephasing delays, was used to measure the decay of the down- and upfield ^{1}H^N doublet components. The weak 90° pulses in the WATERGATE sequence were set to 0.9 ms, yielding an effective bandwidth of ±0.7 ppm around the water where less than 15% of the residual ^{1}H$^\alpha$ spins in the perdeuterated protein are inverted, thereby effectively suppressing ^{1}H–^{1}H *J* modulation during the WATERGATE sequence.

cpd-HSQC

The cpd-HSQC sequence of Ottiger and Bax (*46*) was modified by adding a Rance–Kay style sensitivity enhancement transfer from ^{15}N to ^{1}H^N instead of the reverse INEPT used in the earlier study. Temperature compensation was implemented, as discussed above, in order to ensure that the total amount of RF heating per scan remains constant (*41*).

2D-TROSY

The standard TROSY scheme of Pervushin *et al.* (*37*) was used, but with temperature compensation added. To this extent, a 200-kHz off-resonance irradiation period was added at the end of each FID for the same duration and at the same power as that used for temperature compensation in the first t_1 increment of the complementary cpd-HSQC experiment, described above.

IPAP-HSQC

Separation of downfield and upfield ^{15}N doublet components of interleaved in-phase and antiphase HSQC spectra was accomplished using the IPAP-HSQC method, as described previously (*47*).

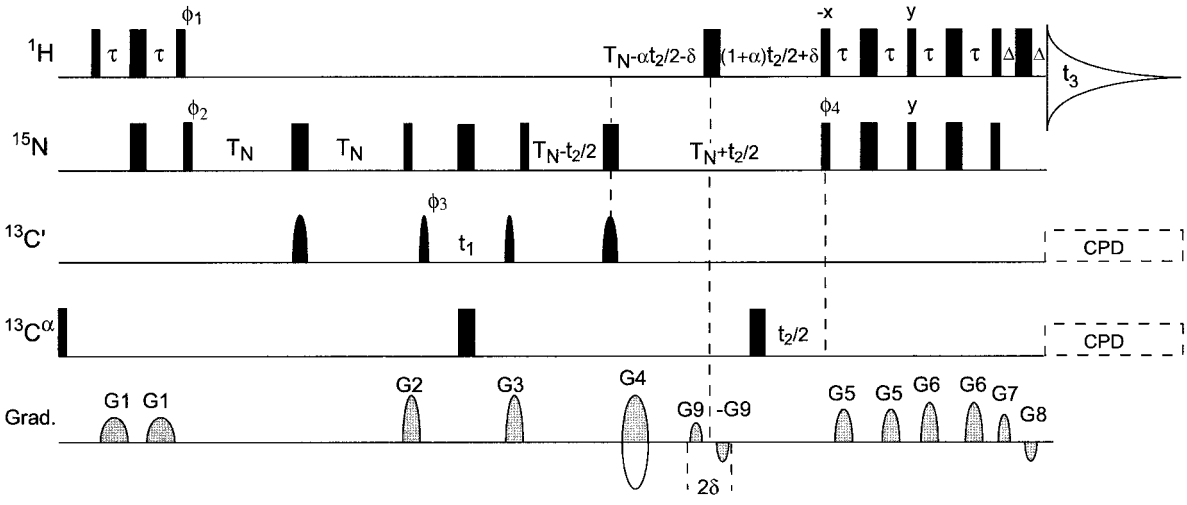

FIG. 2. Three-dimensional *J*-scaled TROSY-HNCO sequence. The scheme is almost identical to the TROSY-HNCO scheme of Fig. 1, but includes an additional ^{1}H 180° pulse during the constant-time ^{15}N evolution period, followed by a 90° ^{1}H pulse, which ensures that it is the upfield (instead of downfield) ^{15}N doublet component that is converted into the upfield $^1H^N$ component, and which also results in a net 180° rotation of the water from $-z$ to $+z$ during the final transfer of magnetization from ^{15}N to $^1H^N$. The experiment can be carried out in the mixed-constant-time mode (Fig. 1) or in the constant-time mode, as shown. The pulse sequence yields an ^{15}N frequency at $\delta_N - \alpha J_{NH}/2$, where J_{NH} denotes the sum of the dipolar and scalar contribution to the splitting. All phase cycling and gradients are the same as for Fig. 1. Antiphase gradients G9 are 600 μs each, with no additional time for gradient recovery (i.e., 2δ = 1.2 ms + τ_{180}, where τ_{180} is the duration of the 180° ^{1}H pulse).

cpd-HNCO

A cpd-HNCO spectrum was recorded using the pulse scheme of Fig. 1. This scheme is essentially identical to the sequence of Kay *et al.* (*40*) except for the use of a semi-constant-time ^{15}N evolution period (*48*) and the use of 180° $^{13}C^\alpha$ pulses instead of SEDUCE-style $^{13}C^\alpha$ decoupling during ^{15}N evolution. Also, temperature compensation was used in order to ensure that the total amount of ^{1}H RF heating per unit of time remains constant throughout the entire pulse scheme.

TROSY-HNCO

TROSY-HNCO spectra were recorded using the scheme of Fig. 1, with the bracketed ^{1}H irradiation and ^{15}N decoupling omitted. This then is the same scheme as that proposed by Yang and Kay (*18*), except that no active flip-back pulse is applied after the first INEPT, and passive radiation damping is used to return H_2O magnetization to the positive *z* axis. Also, semi-constant-time ^{15}N evolution is used and when the data are to be compared with those of the cpd-HNCO experiment, off-resonance ^{1}H irradiation at the end of the acquisition time is used for temperature compensation, such that the average ^{1}H-irradiation per unit of time is the same in the two experiments. When the TROSY-HNCO spectrum is to be compared with the *J*-scaled TROSY-HNCO spectrum (see below), it is recorded without this temperature compensation feature.

J-Scaled TROSY-HNCO

J-scaled TROSY-HNCO spectra were recorded with the pulse scheme of Fig. 2. This pulse scheme is completely analogous to the regular TROSY-HNCO scheme, discussed above, but interchanges the down- and upfield ^{15}N doublet components at time $\delta + (1 + \alpha)t_2/2$ prior to the end of the ^{15}N evolution period. For most of the duration where ^{15}N is transverse ($4T_N - \delta - (1 + \alpha)t_2/2$), however, it relaxes with the favorable ^{15}N downfield doublet component T_2, improving its sensitivity. Note that for longer t_2 durations passive suppression decreases, resulting in a correlation between the downfield ^{15}N doublet component and the downfield $^1H^N$ component. Calculations and experimental results indicate that this peak is 6- to 10-fold weaker than the resonance of interest. If the presence of these weak spurious resonances does present a problem, active suppression using the S^3E approach (*49*) can be used, at the expense of a small cost in signal-to-noise (*17*).

Immediately prior to the $90_{\phi 4}$ ^{15}N pulse, the *J* evolution of the downfield ^{15}N component equals $-J_{NH}[\alpha t_2 + \delta]/2$. The duration of δ is chosen very short (0.6 ms) to accommodate application of gradient pulse G_9, which serves to prevent radiation damping of the inverted water magnetization. The t_2-independent phase, $-J_{NH}\delta/2$, corresponds to a small phase error of approximately 17° in the F_2 dimension of the 3D spectrum, which is easily corrected for during the data processing stage.

For t_2 increments where the delay between the last G_9 and subsequent G_5 gradient pulse becomes longer than about 10 ms, it is beneficial to insert another pair of long, weak gradients of opposite polarity and equal strength between this G_9 gradient and the next 90° ^{15}N pulse. This prevents the onset of radiation damping of the inverted water magnetization.

For proteins with very fast relaxation of the upfield ^{15}N

component, it may be beneficial to use a scaling factor α smaller than 1. For example, if α is set to zero, the ^{15}N resonance appears at its ^{1}H-decoupled position, and the splitting measured relative to TROSY-HNCO equals $J_{NH}/2$. This will increase resolution in the ^{15}N dimension relative to using $\alpha = 1$, but decrease the splitting. In practice, α values smaller than one should be considered if $\exp(-2T_N R_2) < \sim 0.2$, where R_2 refers to the ^{15}N relaxation rate of the upfield ^{15}N doublet component. For such slowly tumbling proteins, it is beneficial for both sensitivity and resolution to adjust α, such that $\exp[-(1 + \alpha)T_N R_2)] \approx 0.2$. As the minimum separation between the 180° ^{15}N and 180° ^{1}H pulse is determined by the duration of gradient G4, the maximum value of α is actually slightly smaller than 1, unless for long t_2 values special precautions are taken in the pulse sequence to switch G4 to a position after the ^{1}H 180° pulse.

RESOLUTION AND SENSITIVITY CONSIDERATIONS

A wide range of different pulse schemes can be used to measure ^{1}H–^{15}N scalar and dipolar couplings. Although splittings can be measured in the ^{1}H^{N} or ^{15}N dimensions, or in hybrids thereof, resolution in hertz (and thereby the accuracy of the measured splitting) is generally best in the ^{15}N dimension (see below). Optimal choice of the pulse scheme also depends strongly on the system to be studied and on the field strength available. Below, the accuracy at which a resonance position can be determined is discussed, and the most important resolution and sensitivity considerations are briefly summarized.

Accuracy of Peak Picking

The accuracy at which a peak position can be determined in the presence of noise was evaluated using simulated, exponentially decaying time domain data in the presence of Gaussian distributed noise. To a good approximation, the accuracy of a peak position was found to increase linearly with the *S/N* ratio, and data presented here correspond to a $S/N = 20$ (peak height divided by the root-mean-squared noise in the frequency domain 2D spectrum). The simulated data consisted of sinusoids decaying exponentially at a range of different rates, ranging from 0 to 3/AT, where AT is the length of the simulated time domain. Data were apodized using the commonly used 60°-shifted sine bell window and subjected to doubling or quadrupling the time domain length prior to Fourier transformation by zero filling.

Figure 3 shows the error in the fitted peak position as a function of the signal decay rate at a constant *S/N*. The error is shown in units of 1/AT, where AT is the length of the time domain in seconds. For example, Fig. 3 indicates that for a constant-time HSQC spectrum with a 28-ms maximum duration of the constant-time evolution, the accuracy at which a peak position can be determined equals 0.033/0.028 = 1.2 Hz, for a *S/N* of 20:1, or 0.6Hz at a *S/N* of 40:1. As can be seen from Fig. 3, the random error increases relatively rapidly with increasing values of the decay rate, reflecting the increase in linewidth.

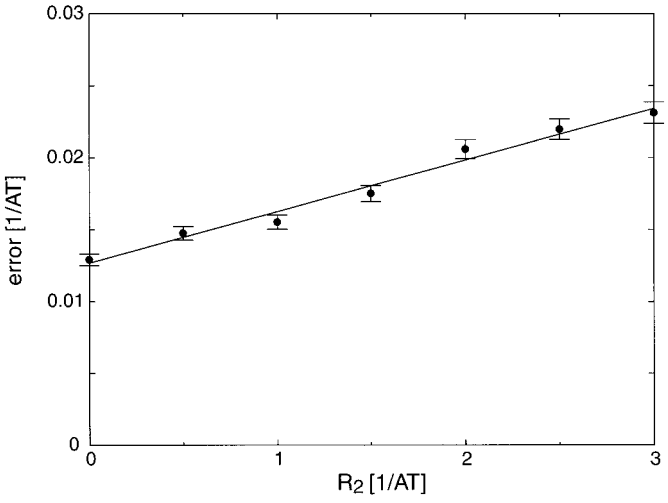

FIG. 3. Uncertainty in peak position in units of $(AT)^{-1}$, for simulated data with a time domain length AT, as a function of the signal decay rate, for a *S/N* of 20:1. The uncertainty represents the standard error in peak position, determined from 500 simulated 2D resonances. Gaussian noise was added in the time domain, and apodization with a 60°-shifted sine-bell window was used. Error bars correspond to the uncertainty divided by $\sqrt{1000}$. For nonoverlapping signals, no significant dependence of the accuracy on the peak picking algorithm was found, with nearly equivalent (within 10%) performance for contour averaging (*59*), Gaussian fitting (*38*), or simple parabolic interpolation (*38*). For parabolic interpolation, no significant improvement was found when increasing the degree of zero filling from two- to fourfold (and increasing the number of frequency domain data points used in the parabolic fit from 3 to 5). For the other two algorithms, performance decreased when using less than fourfold zero filling. The peak position accuracy increases linearly with the *S/N*. This property was used to scale the random uncertainty found in the simulated spectra, so that the graph corresponds to a constant *S/N* level (20:1).

Using Fig. 3 for deriving the accuracy of a given peak position requires that the noise in the vicinity of the peak originates from Gaussian distributed noise in the time domain data and the absence of peak shape or phase distortions in the final spectrum. Phase errors can result in significant shifts in peak position, that to a first approximation are linearly proportional to the magnitude of the phase error and to the linewidth, with an error of 3.2×10^{-3} Hz per degree, per hertz linewidth. Particularly at high *S/N*, errors introduced by such phase distortions may dominate the error introduced by thermal noise.

Resolution considerations. The transverse relaxation rates of the two ^{15}N–{^{1}H} doublet components are $\rho_N \pm \sigma + R_H + R_C$, where ρ_N is the inverse of the transverse relaxation time of in-phase ^{15}N magnetization; σ is the term resulting from relaxation interference between the ^{15}N chemical shift anisotropy and the ^{15}N–^{1}H dipolar interaction (*35, 36*); R_H is the ^{1}H spin flip rate, which is dominated by $J(0)$ spectral density terms and is roughly one-third the value of ρ_N in protonated proteins (*50*),

but much smaller in perdeuterated systems; R_C applies only for ^{13}C-labeled proteins and corresponds to the sum of the intra-residue $^{13}C^{\alpha}$ and preceding $^{13}C^{\alpha}$ and $^{13}C'$ flip rates. Note that these flip rates equal half the corresponding ^{13}C longitudinal relaxation rates. In larger proteins, the ^{13}C longitudinal relaxation rates are typically slow ($\ll 1\ s^{-1}$), and R_C is considerably smaller than R_H in protonated proteins. However, in perdeuterated systems these rates can become comparable. ^{13}C composite pulse decoupling (cpd) can remove the R_C contribution from the ^{15}N linewidth, but was not used in the experiments described in this paper.

Because the cross-correlation rate σ can become close in magnitude to ρ_N, the downfield ^{15}N doublet component (for which ρ_N and σ partially cancel one another) in perdeuterated proteins can be very narrow. In contrast, in protonated proteins the transverse relaxation rate of the downfield component is dominated by R_H, and it therefore exhibits a less dramatic narrowing. In the present study, we experimentally determine the transverse relaxation rates of the upfield and downfield ^{15}N doublet components in several protonated and perdeuterated proteins. This information is essential to optimize simultaneously both spectral resolution and sensitivity.

Sensitivity considerations. The intrinsic sensitivity of a 2D ^{1}H–^{15}N shift correlation experiment is determined by the signal-to-noise that can be obtained for the first increment ($t_1 = 0$) in a given amount of measuring time. If for the regular Rance–Kay enhanced HSQC spectrum (*45*) $S/N = Q$, it would be $Q/2$ for the TROSY spectrum without the Boltzmann enhancement or $Q/2 + B$ for the TROSY spectrum with the ^{15}N Boltzmann factor included (*37*). At equilibrium, and neglecting relaxation losses, $B = Q\ \gamma_N/\gamma_H \approx Q/10$. However, in practice relaxation losses in the first INEPT transfer and faster T_1 relaxation of ^{15}N relative to $^1H^N$, particularly in perdeuterated proteins, results in a significantly larger B/Q ratio. For a protonated protein, a value for $(Q/2 + B)/(Q/2)$ of 1.16 was reported by Pervushin *et al.* (*37*). In proteins where the nonexchangeable protons are deuterated the H^N T_1 can be considerably longer than the ^{15}N T_1 (*51, 52*), and $(Q/2 + B)/(Q/2)$ in such deuterated proteins is expected to be larger, in particular when a relatively short delay (ca. 2 s) is used between consecutive scans. For perdeuterated EIN, we experimentally find values of ca. 1.2.

The sensitivity of a 2D spectrum is directly proportional to the S/N of the first increment, multiplied by $(\sqrt{N})^{-1}\ \Sigma_i \exp[-t_1(i)/T_2]$, where the effect of t_1 apodization is neglected, $t_1(i)$ is the t_1 duration of the ith increment, and a total of N FIDs is collected in the t_1 dimension. Therefore, if for two ^{15}N–^{1}H correlation experiments in which a different ^{15}N T_2 value applies, the t_1 increment is set to a given fraction of the applicable T_2, and the same number of t_1 increments is used in the two experiments (resulting in different spectral widths), the relative sensitivity in the two 2D experiments is directly proportional to the S/N of the spectrum obtained for the first t_1 increment, i.e., to Q for the regular Rance–Kay HSQC, and to $Q/2 + B$ for the Boltzmann-enhanced TROSY. However, the ^{15}N linewidth in the TROSY spectrum will be narrower by a factor $(\rho_N - \sigma + R_H + R_C)/(\rho_N + R_H + R_C)$. The TROSY spectrum yields line narrowing in the ^{1}H dimension too, which, in contrast to the indirectly detected ^{15}N dimension, results in an increase in sensitivity.

For the cpd-HSQC experiment (*46*), the S/N of the first increment equals $Q \exp[-2\delta(\rho_N + R_H + R_C)]$, with $\delta = (2J_{NH})^{-1}$. As ^{15}N magnetization is in-phase with respect to $^1H^N$ during the ^{1}H cpd, R_H does not contribute to its transverse relaxation rate (*50*). In addition, because of the mixed-constant-time nature of the ^{15}N evolution, the apparent rate of ^{15}N decay in the t_1 dimension is reduced by a factor $(1 - 2\alpha)$, with $\alpha = \delta/t_{1max}$. Relative to the regular HSQC, the intrinsic S/N is decreased by $\exp[-2\delta(\rho_N + R_H + R_C)]$, however.

HNCO. For larger proteins, resonance overlap in the 2D HSQC spectrum can considerably reduce the number of amides for which one-bond $^1J_{NH}$ splittings can be measured accurately. The HNCO experiment is the most sensitive triple-resonance experiment and it greatly alleviates the overlap problem by dispersing ^{1}H–^{15}N correlations in the $^{13}C'$ dimension. The narrow downfield ^{15}N–{$^1H^N$} can be obtained using the various variants of the TROSY-HNCO experiment. We prefer to use the simple implementation of Yang and Kay (*18*) in which the broad, upfield ^{15}N–{^{1}H} component is not actively suppressed but is greatly attenuated during the ^{15}N–{$^{13}C'$} de- and rephasing delays (Fig. 1). This experiment does not require selective pulses for water-flip-back and offers the highest S/N. In the absence of $^{13}C'$ decoupling during ^{15}N evolution, sensitivity is twofold lower for the downfield multiplet component compared to the $^{13}C'$-decoupled case, but the presence of $^{13}C'$–^{15}N and $^{13}C'$–$^1H^N$ splittings in this well-resolved spectrum provides important additional couplings (*53*).

Two different approaches can be utilized to obtain information regarding the $^1H^N$ splitting, i.e., to determine the frequency of the other doublet component. First, composite pulse $^1H^N$ decoupling can be used in the ^{15}N dimension (Fig. 1), yielding an intensity $Q \exp[(4T_N - 2\delta)R_H - 4T_N\sigma)/(Q/2 + B)$ relative to the Kay-style TROSY-HNCO (assuming $^{13}C'$ decoupling in both experiments). Second, the J-scaled version of the TROSY-HNCO can be used (Fig. 2), in which the first increment has the same intensity as the regular TROSY-HNCO, but for increasing ^{15}N evolution periods the downfield ^{15}N doublet component is switched with the upfield component for increasing amounts of time. This results in faster ^{15}N decay, but does not affect the intrinsic sensitivity per unit of measuring time, provided that a correspondingly shorter ^{15}N (t_2) acquisition period is used. When the J_{NH} splitting is derived from the difference in ^{15}N frequency in the TROSY-HNCO and cpd-HNCO experiments, the scaling factor is 0.5. When deriving it from TROSY-HNCO and the J-scaled TROSY-HNCO of Fig. 2, the scaling factor is typically close to 1. For larger, perdeuterated proteins, where $Q \exp[(4T_N - 2\delta)R_H - 4T_N\sigma)/(Q/2 +$

TABLE 1
Transverse Decay Times of $^1H^N$-Coupled and -Decoupled ^{15}N Amide Resonances[a]

Protein[c]	ν_H (MHz)	$T_{2,df}$[b] (ms)	$T_{2,uf}$[b] (ms)	$T_{2,cpd}$[b] (ms)	$T_{2,180}$[b] (ms)
EIN-N/C/D	800	131	27	51	52
EIN-N/C/D	600	118	33	60	57
EIN-N	800	79	22	52	35
EIN-N	600	72	28	57	39
UBI-N/C/D	800	200	45	74	74
UBI-N/C/D	600	185	55	93	93
UBI-N/C	800	111	40	73	59
UBI-N/C	600	104	46	87	67
FAB-[Y]-N	800	42	12	27	18

[a] Reported values are the apparent averaged decay constants measured over a τ–180°–τ interval, as described in the text. Random errors, based on duplicate experiments are ca. 4%.

[b] Transverse decay constants for the downfield ($T_{2,df}$) and upfield ($T_{2,uf}$) ^{15}N doublet components measured using HSQC-TROSY, and for the cpd-decoupled ^{15}N resonance ($T_{2,cpd}$) and the 180° (^1H) decoupled ^{15}N resonance ($T_{2,180}$).

[c] EIN, N-terminal domain of Enzyme 1; UBI, ubiquitin; FAB, Fab fragment of antibody. Characters following the three-letter protein name correspond to the nuclei that were isotopically enriched. For FAB-[Y]-N, only the tyrosine residues are ^{15}N enriched.

B) becomes smaller than 1, this latter approach is clearly preferable.

RESULTS AND DISCUSSION

The methods for measurement of ^{15}N–$^1H^N$ couplings were tested for seven samples: $^{15}N/^{13}C$-labeled ubiquitin (76 residues), $^{15}N/^{13}C/^2H$-labeled ubiquitin, ^{15}N-labeled ubiquitin in bicelles, ^{15}N-labeled N-terminal domain of enzyme I (259 residues) in isotropic solution, $^{15}N/^{13}C/^2H$-labeled EIN, both in isotropic solution and in a colloidal suspension of aligned phage particles, and to a FAB fragment of an antibody raised against cholera toxin (440 residues, $M_r = 50$ kDa), in which 19 tyrosine residues were selectively labeled with ^{15}N.

Comparison of ^{15}N Transverse Relaxation Rates

In order to optimize the parameters for measurement of the *J* splittings, knowledge of the approximate transverse relaxation rates of the up- and downfield ^{15}N–{$^1H^N$} doublet components is required. Except for the regular HSQC experiment, T_2 values were measured as described above under Experimental. For EIN, FAB, and protonated ubiquitin, spectra were recorded in the 1D mode, and reported rates correspond to the average over the rates measured for resonances downfield of 8.5 ppm. For measurements in perdeuterated ubiquitin, a "delay-180° (^{15}N)-delay" period preceded the actual ^{15}N evolution period in the 2D TROSY and anti-TROSY experiments, and relaxation for individual resonances was measured as a function of the duration of this period. Results are summarized in Table 1 and confirm that the downfield ^{15}N doublet component has a much longer decay constant than the upfield component. As expected, the ratio of these decay rates increases with magnetic field strength and is much higher for perdeuterated proteins than for fully protonated ones. For the protonated proteins, the T_2 ratio at 800 MHz ^1H frequency is about 3.2, and this drops to ca 2.4 at 600 MHz. For both perdeuterated ubiquitin and perdeuterated EIN, these ratios are considerably larger, yielding an average ratio of 4.8 at 800 MHz and 3.5 at 600 MHz. For ubiquitin, the decay rates and their ratios are

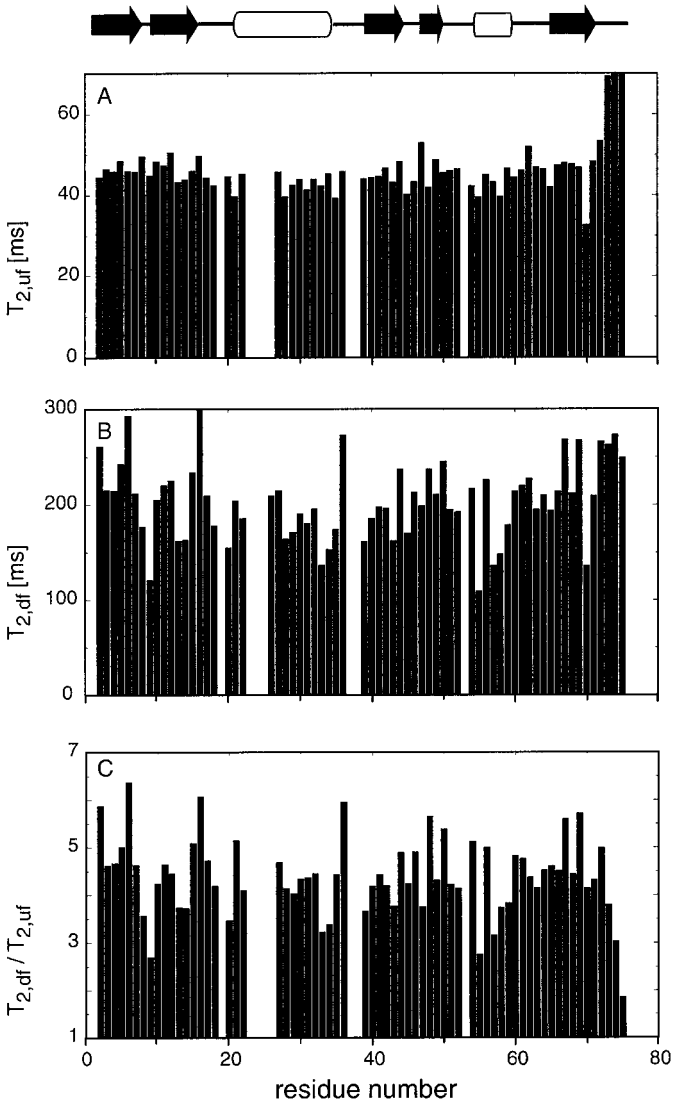

FIG. 4. Effective transverse decay times of the backbone ^{15}N doublet components in $^2H/^{13}C/^{15}N$ ubiquitin at 7° ($\tau_c = 7.0$ ns), as measured by a Hahn echo experiment at 800-MHz ^1H frequency (see text). (A) Upfield ^{15}N–{^1H} doublet component; (B) downfield ^{15}N–{^1H} doublet component; (C) ratio of the transverse decay times of the downfield and upfield ^{15}N decay times. Random errors in the rates are estimated to be less than 3%. Ubiquitin's secondary structure is marked schematically above A. C-terminal residues 73–76 are highly mobile.

shown as a function of residue number in Fig. 4. Clearly, there is a wide range of variation in the decay rate of the narrow component (185 ± 30 ms at 600 MHz; 200 ± 40 ms at 800 MHz), whereas the upfield component shows a much more homogeneous behavior (55 ± 4 ms at 600 MHz; 45 ± 3 ms at 800 MHz). This can be rationalized by the fact that decay of the narrow component is dominated by $\rho - \sigma$, whereas the upfield decay is dominated by $\rho + \sigma$. As ρ and σ are of comparable magnitude, a small fluctuation in σ (corresponding to a variation in the orientation or magnitude of the ^{15}N CSA tensor) causes a much larger fractional change in $\rho - \sigma$ than in $\rho + \sigma$. Also, conformational and hydrogen exchange contributions to the transverse relaxation rate, which have the same absolute magnitude for both doublet components, have a much larger fractional effect on the slowest relaxing component.

As expected, the effective ^{15}N decay rate measured in the 180° refocused regular HSQC experiment corresponds closely to the average of those of the upfield and downfield doublet components (Table 1). Compared to this refocused regular HSQC experiment, the ^{15}N decay rate measured in the cpd-HSQC experiment is ca. 30% longer in the protonated samples, but virtually unchanged for the perdeuterated proteins.

Comparison of $^1H^N$ Decay Rates

In protonated proteins, the ^{1}H T_2 is dominated by homonuclear dipolar interactions and is therefore much shorter than the ^{15}N T_2 of backbone amides. In highly perdeuterated proteins, however, the $^1H^N$ T_2 is dominated by the ^{15}N–$^1H^N$ dipolar interaction (*54*) and much narrower linewidths can be obtained. As it potentially could be advantageous to measure ^{1}H–^{15}N dipolar splittings in the ^{1}H dimension, we also have measured the transverse decay rates of the two $^1H^N$–{^{15}N} doublet components in $^{15}N/^{13}C/^2H$-labeled ubiquitin. Results recorded at 800 MHz are shown in Fig. 5. On average, at 800 MHz the decay rate for the narrow, upfield doublet components is 1.77 ± 0.38 times slower than for the downfield component but a substantial degree of variation is seen. In particular, inspection of Fig. 5 shows that for α-helical residues the narrowing of the upfield doublet component is much smaller than for those in the β-sheet. This agrees with earlier measurements, which indicate that the relaxation interference between H^N CSA and $^1H^N$–^{15}N dipolar interactions is, on average, smaller in helices than in the β-sheet (*55*, *56*). As was the case for ^{15}N, the broad $^1H^N$–{^{15}N} doublet component shows remarkably homogeneous relaxation rates (49 ± 6 ms at 600 MHz; 44 ± 7 ms at 800 MHz), whereas a much wider range of rates (78 ± 22 ms at 600 MHz; 80 ± 24 ms at 800 MHz) is observed for the narrower, upfield component. Although in perdeuterated proteins the broadest ^{1}H doublet component relaxes at a rate comparable to the broadest ^{15}N doublet component, in aligned samples further $^1H^N$ line broadening results from unresolved homonuclear $^1H^N$–$^1H^N$ dipolar couplings, whereas heteronuclear ^{15}N–^{1}H dipolar couplings are much smaller. Together

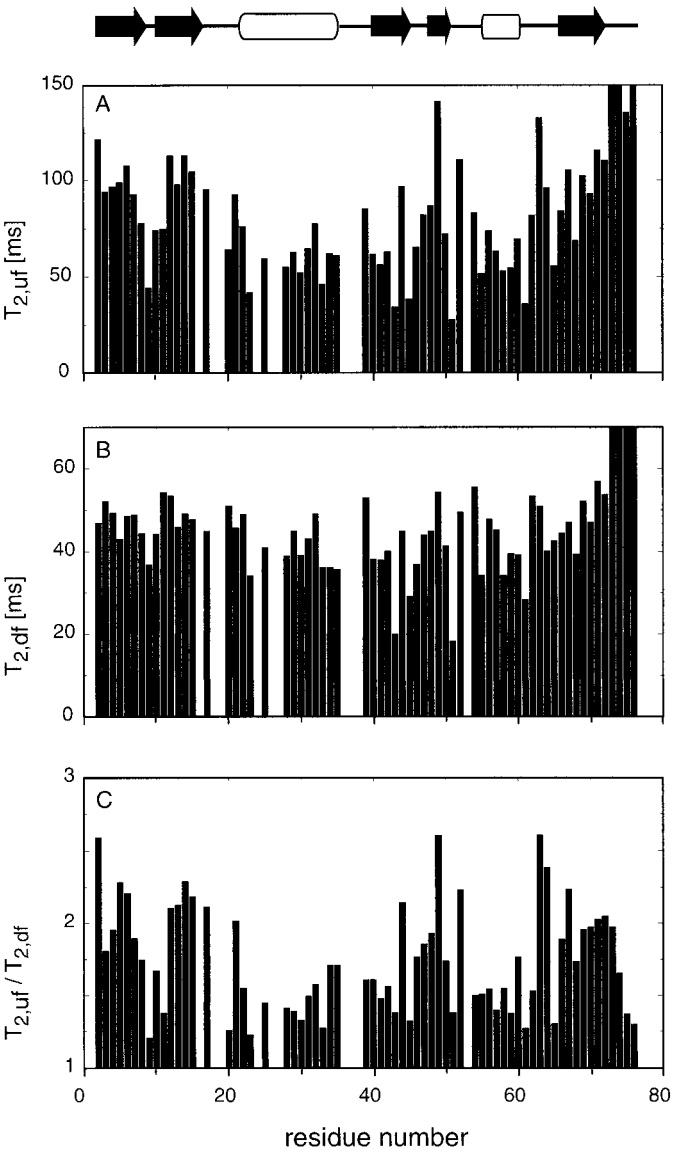

FIG. 5. Effective transverse decay times of the backbone $^1H^N$ doublet components in $^2H/^{13}C/^{15}N$ ubiquitin at 7° (τ_c = 7.0 ns), as measured by a Hahn echo experiment at 800-MHz ^{1}H frequency (see text). (A) Upfield $^1H^N$–{^{15}N} doublet component; (B) downfield $^1H^N$–{^{15}N} doublet component; (C) ratio of the transverse decay times of the upfield and downfield $^1H^N$ decay times. Random errors in the rates are estimated to be less than 3%.

with the very narrow linewidth of the downfield ^{15}N component relative to the upfield $^1H^N$ component, this makes it preferable to measure ^{15}N–$^1H^N$ splittings in the ^{15}N dimension.

Measurement of ^{15}N–$^1H^N$ splittings. For ^{15}N-labeled ubiquitin in bicelles, comparison of the NH splittings ($^1J_{NH}$ + $^1D_{NH}$) obtained by the IPAP-HSQC method with twice the difference between the ^{15}N frequency in the TROSY and the cpd-HSQC spectra yields good agreement, with a pairwise rmsd of 0.6 Hz and no apparent systematic errors (data not shown). When attempting to calculate the $^1J_{NH}$ + $^1D_{NH}$ value

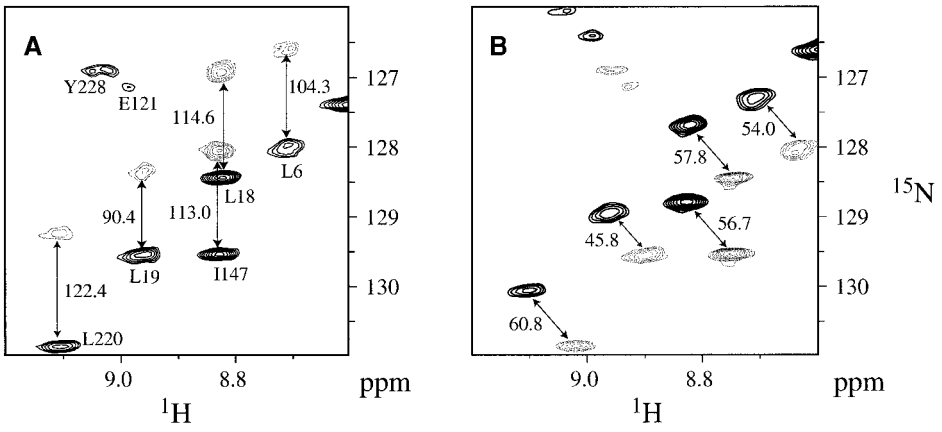

FIG. 6. Small regions of ^{1}H–^{15}N HSQC correlation spectra of the EIN, in a colloidal suspension of filamentous bacteriophage *fd*. Spectra are recorded at 750 MHz and 40°. All spectra were apodized with 63°-shifted sine-bell squared windows in the ^{1}H^N dimension and a 63°-shifted sine-bell window in the ^{15}N dimension. (A) IPAP-HSQC-spectrum (*45*), recorded with a t_1 (^{15}N) acquisition time of 100 ms and a t_2 (^{1}H^N) acquisition time of 77 ms. The spectra containing the downfield (thick contours) and upfield (thin contours) doublet components are superimposed. Optimum separation of the upfield and downfield components was achieved using a scaling factor for the antiphase EIN spectrum relative to the in-phase HSQC spectrum of 1.18. (B) Superposition of the cpd-HSQC and TROSY-HSQC spectra. The acquisition times were 100 ms in t_1 (^{15}N) and 77 ms in t_2 for cpd-HSQC, and 130 ms (t_1) and 100 ms (t_2) for TROSY-HSQC. The ^{15}N–^{1}H^N splittings (in hertz) are marked together with the sequential assignment. Splittings marked in B correspond to measured displacement in the ^{15}N dimension; due to the larger linewidth in the ^{1}H^N dimension, the random uncertainty in the relative displacement in the ^{1}H dimension is considerably larger.

from frequencies measured in the ^{1}H dimension of the TROSY and the cpd-HSQC spectra, the pairwise rmsd relative to the IPAP splittings is considerably larger (3.1 Hz), which corresponds to an rms error of 1.1 Hz in the determination of the ^{1}H resonance frequency of individual peaks. This larger error reflects the large linewidth in the ^{1}H^N dimension of the aligned sample, which is dominated by mostly unresolved ^{1}H–^{1}H dipolar couplings in this nondeuterated protein and which adversely affects the accuracy of peak picking.

When applied to phage-oriented ^{2}H/^{15}N/^{13}C-EIN at 750 MHz, the resulting IPAP-HSQC subspectra, corresponding to the downfield and upfield ^{15}N–{^{1}H^N} doublet components, differ greatly in ^{15}N linewidth and intensity (Fig. 6A). As discussed before, this results from cross correlation between the ^{1}H–^{15}N dipolar and ^{15}N CSA relaxation mechanisms. On average, the upfield component is about twofold weaker and broader than the downfield multiplet component, resulting in an approximately fourfold increase in the uncertainty of its peak position relative to the downfield component. So, if the uncertainty in the downfield peak position is U, the uncertainty in the upfield position is $4U$, and the random error in the splitting is $U\sqrt{17}$. Resolution of the downfield component is limited by the acquisition parameters used in the t_1 dimension and could be improved by longer sampling in the t_1 dimension. However, as the uncertainty in the splitting is already dominated by the error in the peak position of the upfield component, longer t_1 acquisition would not improve the accuracy of the measured splitting.

The two doublet components, measured separately in the mixed-constant-time cpd-HSQC and TROSY spectra (Fig. 6B) have comparable *S/N*, and the ^{15}N linewidth in the cpd-HSQC spectrum is only about 1.3 times larger than in the TROSY spectrum, resulting in a 1.3 times larger uncertainty in peak position. The *S/N* ratio for the TROSY and the cpd-HSQC spectra is about 20% higher than for the downfield IPAP-HSQC component (total measuring time for cpd-HSQC plus TROSY-HSQC equals that of the IPAP-HSQC data set), resulting in an uncertainty in the measured half-splitting of $U(1 + 1.3^2)^{1/2}/1.2 \approx 1.4U$, or an rms error of $2.8U$ in the full splitting. So, despite the fact that the ^{15}N splitting measured in the cpd-HSQC relative to the TROSY spectrum is only $(^1J_{NH} + {}^1D_{NH})/2$, instead of $(^1J_{NH} + {}^1D_{NH})$ in the IPAP-HSQC experiment, for larger proteins the accuracy of $(^1J_{NH} + {}^1D_{NH})$ is somewhat better than for the IPAP-HSQC method. Also, the narrower linewidth in the cpd-HSQC spectrum relative to that of the upfield component in the IPAP-HSQC spectrum reduces spectral overlap. The pairwise rmsd of the two sets of measured dipolar couplings is 1.76 Hz (Fig. 7A), indicating that the error in the dipolar coupling from the TROSY/cpd-HSQC method is ca. 1 Hz.

The dipolar NH couplings define the molecular alignment tensor. Due to partial proteolysis of the C-terminal tail of the phage containing EIN sample and resulting extensive spectral overlap, only a limited number of dipolar couplings could be obtained from the 2D spectra. Figure 7B shows a plot of the measured dipolar couplings versus those predicted on the basis of a 2.5 Å crystal structure (pdb code 1ZYM) (*57*). Comparison of Figs. 7A and 7B shows that the accuracy of the measurement is much better than the agreement between the measured data and those predicted by this relatively low resolution X-ray structure. Therefore, the accuracy of the dipolar coupling measurement is fully sufficient for use in structure calculation.

For larger proteins, spectral overlap in the 2D HSQC or TROSY spectra limits the number of residues for which $^1D_{NH}$

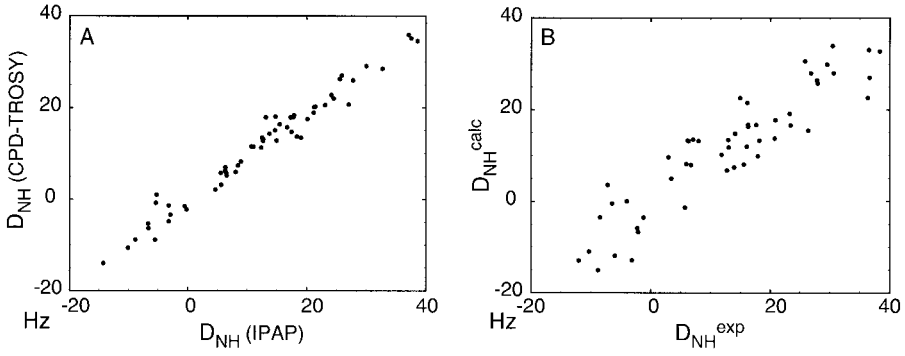

FIG. 7. Comparison of dipolar couplings in EIN. (A) Correlation between the dipolar couplings obtained from the IPAP-HSQC spectrum versus values obtained from TROSY-HSQC and cpd-HSQC data sets (see Fig. 6). The pairwise rmsd equals 1.76 Hz; the correlation coefficient R equals 0.984. As discussed in the text, the IPAP-HSQC data have larger random uncertainty than those derived from TROSY-HSQC/cpd-HSQC. (B) Experimental dipolar couplings, obtained from TROSY-HSQC-/cpd-HSQC, versus couplings predicted from its 2.5-Å resolution X-ray crystal structure (*57*; pdb code 1ZYM).

can be measured and couplings are more conveniently obtained from 3D HNCO spectra. As the ^{15}N magnetization evolves during the mixed-constant-time ^{15}N evolution period, t_2 (Fig. 1), the decay for the last t_2 increment corresponds to $\exp[-(t_{2\max} - 2T_N)/T_2]$, where $2T_N$ is the ^{15}N–^{13}C de-/rephasing duration (33 ms) and T_2 is the applicable decay constant for the TROSY- and CPD-decoupled in-phase ^{15}N magnetization. ^{13}C′ T_2 relaxation is relatively rapid, particularly at high field strengths. Together with the rather narrow spectral window covered by the ^{13}C′ resonances, a relatively small number of t_1 increments (32 in our experiments) is needed, therefore. However, because of the rather long H^N T_1 in perdeuterated proteins, and the requirement for a two-step phase cycle for artifact suppression, the maximum number of t_2 increments that can be covered in a typical 24-h measurement is limited. Data reported here were recorded as 32* × 64* × 768* (cpd-HNCO) and 32* × 100* × 768* (TROSY-HNCO) matrices.

Figure 8 shows superimposed small ^{1}H–^{15}N cross sections from 3D cpd-HNCO and TROSY-HNCO spectra of EIN in isotropic solution (A, C, E) and in the aligned phage medium (B, D, F), taken at the ^{13}C′ chemical shifts of A101, A102, and A103. On average, after correcting for the 1.6 times longer measuring time of the TROSY-HNCO spectrum relative to the cpd-HNCO, its *S/N* ratio remains approximately 1.3 ± 0.3 times higher than for the cpd-HNCO spectrum. This confirms that for larger, perdeuterated proteins TROSY-HNCO is intrinsically more sensitive per unit of time than the cpd-HNCO experiment. Next to the narrower $^1H^N$ linewidth in TROSY-HNCO, the longer t_2 of the downfield ^{15}N doublet component compared to the cpd-decoupled ^{15}N resonance, applicable during the relatively long ^{15}N–{^{13}C′} de- and rephasing periods, is primarily responsible for this increase in *S/N* (*15–18*). Combined, the TROSY-HNCO and cpd-HNCO experiments provide an effective and sensitive method for measuring the one-bond ^{1}H–^{15}N dipolar couplings in larger proteins with reasonable accuracy.

For perdeuterated proteins which are also ^{15}N- and ^{13}C-enriched, it can be advantageous to use the TROSY-HNCO experiment to record the narrow ^{15}N doublet component with very high resolution, in such a way that it can also be used to measure $^1J_{C'N}$ and $^2J_{C'HN}$ splittings. Clearly, it is not necessary (and frequently impossible) to resolve the small $^1J_{C'N}$ splitting when recording separately the upfield ^{15}N doublet component.

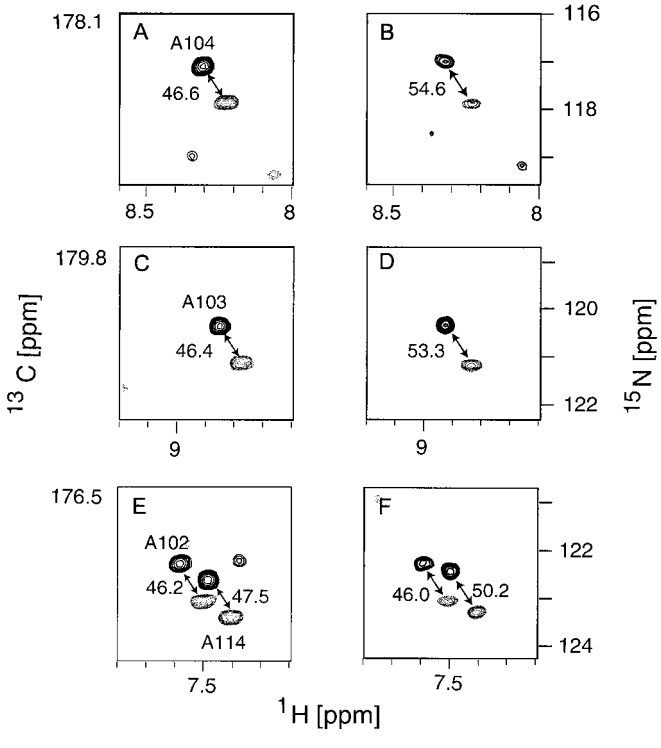

FIG. 8. Small sections showing superimposed small regions from the 3D cpd-HNCO spectrum (thick contours) and TROSY-HNCO spectrum (thin contours) of ^{2}H/^{13}C/^{15}N EIN in isotropic phase (A,C,E) and in the *fd* solution (B,D,F), recorded at 600-MHz ^{1}H frequency. The acquisition times were 21 ms in t_1 (^{13}C′), 51 ms in t_2 (^{15}N), and 45 ms in t_3 for cpd-HNCO, and 21 ms in t_1 (^{13}C′), 80 ms in t_2 (^{15}N) and 45 ms in t_3 for TROSY-HNCO. Both spectra were apodized with 63°-shifted sine-bell squared windows in the $^1H^N$ dimension and a 63°-shifted sine-bell window in the ^{15}N and ^{13}C dimension.

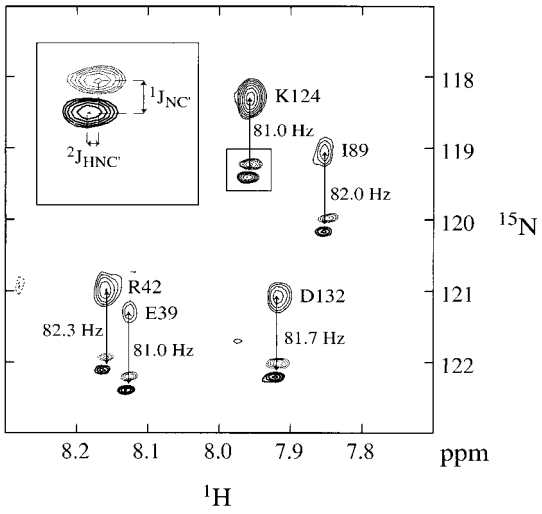

FIG. 9. Superposition of small sections taken from the 3D TROSY-HNCO and 3D *J*-scaled TROSY-HNCO spectrum of EIN in the isotropic phase, recorded at 800-MHz ^{1}H frequency. The acquisition times were 16 ms in t_1 (^{13}C′), and 92 ms in t_3 for both spectra, and 115 ms in t_2 (^{15}N) for TROSY-HNCO and 33 ms for *J*-scaled TROSY-HNCO. Both spectra were apodized with 63°-shifted sine-bell squared windows in the ^{1}H^N dimension and a 63°-shifted sine-bell window in the ^{15}N and ^{13}C dimension. No ^{13}C′ decoupling was used during ^{15}N evolution of the TROSY-HNCO spectrum, resulting in the antiphase doublet pattern for the downfield ^{15}N–{^{1}H} doublet component, from which $^1J_{C'N}$ and $^2J_{C'HN}$ can be measured (see inset). The *J*-scaled TROSY-HNCO spectrum (scaling factor $\alpha = 0.748$) is recorded with ^{13}C′ decoupling during ^{15}N evolution. ^{15}N–{^{1}H} *J* splittings are scaled by $(1+\alpha)/2 = 0.874$.

This is illustrated in Fig. 9, for superimposed small regions of the 3D TROSY-HNCO (pulse sequence of Fig. 1) and *J*-scaled TROSY-HNCO spectra (pulse sequence of Fig. 2). No attempt is made to resolve these splittings when optimizing the pulse scheme for detection of the upfield doublet component, which utilizes a much shorter acquisition time in the t_2 (^{15}N) dimension than the regular TROSY-HNCO spectrum. The scaling factor α employed in the *J*-scaled TROSY-HNCO experiment was 0.748, and the splittings marked in Fig. 9 correspond to $(1 + \alpha)/2 = 87.4\%$ of the true $^1J_{NH}$ splittings. The $^1J_{C'N}$ and $^2J_{C'HN}$ are not scaled.

It should be pointed out that the above discussed sensitivity gain in TROSY-HSQC and TROSY-based 3D experiments applies to perdeuterated proteins. For fully protonated proteins at high magnetic field strength, the proton spin-flip rate, R_H, dominates the transverse relaxation rate of the ^{15}N downfield doublet component. The increase in the TROSY ^{15}N decay constant relative to the CPD-decoupled ^{15}N signal (which is not affected by R_H) is therefore much smaller (Table 1) and does not necessarily offset the smaller amount of magnetization available after the first INEPT transfer.

CONCLUDING REMARKS

The ^{15}N decay rates in the TROSY, HSQC, and cpd-HSQC spectra are all dominated by *J(0)* spectral density terms. Their ratios are, therefore, to a good approximation, independent of the rotational correlation time, and results reported here can be readily extrapolated to any other protein for which the approximate rotational correlation time is known.

Comparison of relaxation rates of the two ^{15}N–{^{1}H} doublet components and the cpd-decoupled and regular HSQC experiments shows distinctly different results for protonated proteins and proteins in which the nonexchanging hydrogens are substituted by deuterium. In these deuterated proteins, ^{1}H–^{1}H spin-flip rates are low and do not contribute very much to the transverse relaxation of the ^{15}N doublet components. As a result of relaxation interference, the downfield and upfield doublet components differ in transverse relaxation rate by a factor of 4.8 ± 0.8 for perdeuterated EIN at 800 MHz and 3.6 ± 0.5 at 600 MHz. For perdeuterated ubiquitin, the ratios are 4.5 ± 0.8 at 800 MHz and 3.4 ± 0.5 at 600 MHz. The cpd-decoupled and regular HSQC ^{15}N decay rates are nearly identical and correspond to the average decay rate of the two doublet components. In fully protonated proteins the doublet components differ in transverse relaxation rate by a factor of 3.6 for EIN at 800 MHz and 2.6 at 600 MHz, and for ubiquitin, the ratios are 2.8 (800 MHz) and 2.3 (600 MHz). The regular HSQC ^{15}N decay rate again corresponds to the average of the two doublet components, but the cpd-decoupled in-phase ^{15}N magnetization exhibits a 25% slower transverse relaxation rate. The mixed-constant-time nature of the evolution period in the cpd-decoupled HSQC experiment offers an additional period of $1/J_{NH}$ of decay-free evolution, decreasing the apparent ^{15}N decay rate even further.

The intensity of the first increment of the 2D ^{1}H–^{15}N correlation spectrum, which determines the integrated intensity of the corresponding correlation in the 2D spectrum, is highest for the regular HSQC spectrum and approximately 40% lower for the TROSY spectrum. Compared to the regular HSQC spectrum, the first increment of the cpd-decoupled HSQC spectrum (which includes an additional ^{15}N decay period of duration of $1/J_{NH}$) is weaker by 10% for the rapidly tumbling ubiquitin ($\tau_c = 7$ ns at 7°, and by nearly 50% for the much larger Fab ($\tau_c \approx 23$ ns). These ratios are not much affected by whether the protein is protonated or deuterated.

We have demonstrated that accurate ^{1}H–^{15}N dipolar couplings in weakly aligned proteins can be measured from the difference in ^{15}N frequency in a TROSY-HSQC spectrum and a cpd-HSQC spectrum, provided that proper compensation is made for the differential radiofrequency heating in the two experiments. For perdeuterated proteins, the ^{15}N transverse decay rates in the cpd-decoupled and the regular HSQC experiment are very similar. For these proteins the regular ^{1}H–^{15}N HSQC, including Rance–Kay sensitivity enhancement (*45*) and a ^{1}H 180° pulse for decoupling in the t_1 dimension, is therefore preferred because of its inherently slightly higher sensitivity and the absence of a need for temperature compensation. For larger proteins, the accuracy at which ^{1}H–^{15}N dipolar couplings can be measured from the ^{1}H–^{15}N TROSY-HSQC and the

regular HSQC (cpd-HSQC for protonated proteins) surpasses that of the IPAP-HSQC approach. The approach is readily extended to 3D NMR experiments such as HNCO, where the combination of TROSY-HNCO and mixed-constant-time cpd-HNCO provides two spectra with adequate sensitivity and resolution. For perdeuterated proteins, the combined recording of the TROSY-HNCO and the *J*-scaled TROSY-HNCO spectra provides the most attractive method to measure the $^{1}H–^{15}N$ splittings. If the TROSY-HNCO spectrum is recorded at high ^{15}N resolution, this permits simultaneous measurement of one-bond $^{13}C'–^{15}N$ and two-bond $^{13}C'–^{1}H^{N}$ splittings too.

ACKNOWLEDGMENTS

We thank Dan Garrett for making available to us the resonance assignments of EIN, Jacob Anglister for the sample of ^{15}N[Y]-Fab, and Stephan Grzesiek and Marco Rogowski for the $^{2}H/^{13}C/^{15}N$–ubiquitin sample. G.K. is the recipient of a Erwin Schrödinger fellowship (J-1706MOB) of the Austrian Foundation for Advancement of Scientific Research. This work was supported by the AIDS Targeted Anti-Viral Program of the Office of the Director of the National Institutes of Health.

REFERENCES

1. J. L. Markley, I. Putter, and O. Jardetzky, High resolution nuclear magnetic resonance spectra of selectively deuterated staphylococcal nuclease, *Science* **161,** 1249–1251 (1968).
2. D. M. LeMaster and F. M. Richards, NMR sequential assignment of *Escherichia-coli* thioredoxin utilizing random fractional deuteration, *Biochemistry* **27,** 142–150 (1988).
3. D. Marion, P. C. Driscoll, L. E. Kay, P. T. Wingfield, A. Bax, A. M. Gronenborn, and G. M. Clore, Overcoming the overlap problem in the assignment of ^{1}H NMR spectra of larger proteins using three-dimensional homonuclear Hartmann–Hahn and nuclear Overhauser-$^{1}H–^{15}N$ heteronuclear multiple quantum coherence spectroscopy, *Biochemistry* **28,** 6150–6156 (1989).
4. M. Ikura, L. E. Kay, and A. Bax, A novel approach for sequential assignment of ^{1}H, ^{13}C and ^{15}N spectra of larger proteins; Heteronuclear triple-resonance NMR spectroscopy. Application to calmodulin. *Biochemistry* **29,** 4659 (1990).
5. S. Grzesiek, J. Anglister, H. Ren, and A. Bax, ^{13}C line narrowing by ^{2}H decoupling in $^{2}H/^{13}C/^{15}N$–enriched proteins. Applications to triple resonance 4D *J*-connectivity of sequential amides, *J. Am. Chem. Soc.* **115,** 4369–4370 (1993).
6. T. Yamazaki, W. Lee, C. H. Arrowsmith, D. R. Muhandiram, and L. E. Kay, A suite of triple resonance NMR experiments for the backbone assignment of ^{15}N, ^{13}C, ^{2}H labeled proteins with high sensitivity, *J. Am. Chem. Soc.* **116,** 11655–11666 (1994).
7. K. H. Gardner, M. K. Rosen, and L. E. Kay, Global folds of highly deuterated, methyl protonated proteins by multidimensional NMR, *Biochemistry* **36,** 1389–1401 (1997).
8. G. M. Clore and A. M. Gronenborn, NMR structures of proteins and protein complexes beyond 20,000 Mr, *Nat. Struct. Biol.* **4**(Suppl. S), 849–853 (1997).
9. K. Pervushin, R. Riek, G. Wider, and K. Wüthrich, Attenuated T_2 relaxation by mutual cancellation of dipole-dipole coupling and chemical shift anisotropy indicates an avenue to NMR structures of very large biological macromolecules in solution, *Proc. Natl. Acad. Sci. USA* **94,** 12366–12371 (1997).
10. T. Yamazaki, T. Otomo, N. Oda, Y. Kyogoku, K. Uegaki, N. Ito, Y. Ishino, and H. Nakamura, Segmental isotope labeling for protein NMR using peptide splicing, *J. Am. Chem. Soc.* **120,** 5591–5592 (1998).
11. R. Xu, B. Ayers B, D. Cowburn, and T. W. Muir, Chemical ligation of folded recombinant proteins: Segmental isotopic labeling of domains for NMR studies, *Proc. Natl. Acad. Sci. USA* **96,** 388–393 (1999).
12. R. A. Venters, B. T. Farmer, C. A. Fuerke, and L. D. Spicer, Characterizing the use of perdeuteration in NMR studies of large proteins: ^{13}C, ^{15}N and ^{1}H assignments of human carbonic anhydrase II, *J. Mol. Biol.* **264,** 1101–1116 (1996).
13. X. Shan, K. H. Gardner, D. R. Muhandiram, N. S. Rao, C. H. Arrowsmith, and L. E. Kay, Assignment of ^{15}N, $^{13}C^{\alpha}$, $^{13}C^{\beta}$ and HN resonances in an ^{15}N, ^{13}C, ^{2}H labeled 64 kDa trp repressor–operator complex using triple resonance NMR spectroscopy and ^{2}H-decoupling, *J. Am. Chem. Soc.* **118,** 6570–6579 (1996).
14. K. H. Gardner, X. C. Zhang, K. Gehring, and L. E. Kay, Solution NMR studies of a 42 KDa *Escherichia coli* maltose binding protein beta-cyclodextrin complex: Chemical shift assignments and analysis, *J. Am. Chem. Soc.* **120,** 11738–11748 (1998).
15. M. Salzmann, K. Pervushin, G. Wider, H. Senn, and K. Wüthrich, TROSY in triple-resonance experiments: New perspectives for sequential NMR assignment of large proteins. *Proc. Natl. Acad. Sci. USA* **95,** 13585–13590 (1998).
16. M. Salzmann, K. Pervushin, G. Wider, H. Senn, and K. Wüthrich, TROSY-type triple-resonance experiments for sequential NMR assignments of large proteins, *J. Am. Chem. Soc.* **121,** 844–848 (1999).
17. D. W. Yang and L. E. Kay, TROSY triple-resonance four-dimensional NMR spectroscopy of a 46 ns tumbling protein, *J. Am. Chem. Soc.* **121,** 2571–2575 (1999)
18. D. W. Yang and L. E. Kay, Improved ^{1}HN-detected triple resonance TROSY-based experiments, *J. Biomol. NMR* **13,** 3–10 (1999).
19. L. E. Kay and K. H. Gardner, Solution NMR spectroscopy beyond 25 kDa, *Curr. Opin. Struct. Biol.* **7,** 722–731 (1997).
20. J. R. Tolman, J. M. Flanagan, M. A. Kennedy, and J. H. Prestegard, Nuclear magnetic dipole interactions in field-oriented proteins—Information for structure determination in solution, *Proc. Natl. Acad. Sci. USA* **92,** 9279–9283 (1995).
21. H. C. King, K. Y. Wang, I. Goljer, and P. H. Bolton, Magnetic alignment of duplex and quadruplex DNAs, *J. Magn. Reson. B* **109,** 323–325 (1995).
22. N. Tjandra, S. Grzesiek, and A. Bax, Magnetic field dependence of nitrogen–proton *J* splittings in ^{15}N-enriched human ubiquitin resulting from relaxation interference and residual dipolar coupling. *J. Am. Chem. Soc.* **118,** 6264–6272 (1996).
23. N. Tjandra, J. G. Omichinski, A. M. Gronenborn, G. M. Clore, and A. Bax, Use of dipolar $^{1}H–^{15}N$ and $^{1}H–^{13}C$ couplings in the structure determination of magnetically oriented macromolecules in solution. *Nat. Struct. Biol.* **4,** 732–738 (1997).
24. G. M. Clore, M. R. Starich, C. H. Bewley, M. Cai, and J. Kuszewski, Impact of residual dipolar couplings on the accuracy of NMR structures determined form a minimal number of NOE constraints, *J. Am. Chem. Soc.* **121,** 6513–6514 (1999).
25. C. R. Sanders and J. P. Schwonek, Characterization of magnetically orientable bilayers in mixtures of dihexanoyl phosphatidylcholine and dimyristoyl phosphatidylcholine by solid-state NMR. *Biochemistry* **31,** 8898–8905 (1992).
26. R. R. Vold and R. S. Prosser, Magnetically oriented phospholipid

bilayered micelles for structural studies of polypeptides. Does the ideal bicelle exist? *J. Magn. Reson. B* **113,** 267–271 (1996).

27. A. Bax and N. Tjandra, High resolution NMR of human ubiquitin in an aqueous liquid crystalline medium, *J. Biomol. NMR* **10,** 289–292 (1997).

28. N. Tjandra and A. Bax, Direct measurement of distances and angles in biomolecules by NMR in a dilute liquid crystalline medium. *Science* **278,** 1111–1114 (1997).

29. M. Ottiger and A. Bax, Characterization of magnetically oriented phospholipid micelles for measurement of dipolar couplings in macromolecules. *J. Biomol. NMR* **12,** 361–372 (1998).

30. G. M. Clore, M. R. Starich, and A. M. Gronenborn, Measurement of residual dipolar couplings of macromolecules aligned in the nematic phase of a colloidal suspension of rod-shaped viruses, *J. Am. Chem. Soc.* **120,** 10571–10572 (1998).

31. M. R. Hansen, L. Mueller, and A. Pardi, Tunable alignment of macromolecules by filamentous phage yields dipolar coupling interactions, *Nat. Struct. Biol.* **5,** 1065–1074 (1998).

32. R. S. Prosser, J. A. Losonczi, and I. V. Shiyanovskaya, *J. Am. Chem. Soc.* **120,** 11010–11011 (1998).

33. B. W. Koenig, J-S Hu, M. Ottiger, S. Bose, R. W. Hendler, and A. Bax, NMR measurement of dipolar couplings in proteins aligned by transient binding to purple membrane fragments, *J. Am. Chem. Soc.* **121,** 1385–1386 (1999).

34. J. Sass, F. Cordier, A. Hoffmann, M. Rogowski, A. Cousin, J. G. Omichinski, H. Loewen, and S. Grzesiek, Purple Membrane Induced Alignment of Biological Macromolecules in the Magnetic Field, *J. Am. Chem. Soc.* **121,** 2047–2055 (1999).

35. M. Goldman, Interference effects in the relaxation of a pair of unlike spin-1/2 nuclei, *J. Magn. Reson.* **60,** 437–452 (1984).

36. N. Tjandra, A. Szabo, and A. Bax, Protein backbone dynamics and ^{15}N chemical shift anisotropy from quantitative measurement of relaxation interference, *J. Am. Chem. Soc.* **118,** 6986–6991 (1996).

37. K. V. Pervushin, G. Wider, and K. Wüthrich, Single transition-to-single transition polarization transfer (ST2-PT) in [^{15}N, ^{1}H]-TROSY. *J. Biomol. NMR,* **12,** 345–348 (1998).

38. F. Delaglio, S. Grzesiek, G. W. Vuister, G. Zhu, J. Pfeifer, and A. Bax, NMRPipe: A multidimensional spectral processing system based on UNIX pipes, *J. Biomol. NMR.* **6,** 277–293 (1995).

39. S. Grzesiek and A. Bax, The importance of not saturating H_2O in protein NMR. Application to sensitivity enhancement and NOE measurements. *J. Am. Chem. Soc.* **115,** 12593–12594 (1993).

40. L. E. Kay, G. Y. Xu, and T. Yamazaki, Enhanced sensitivity triple resonance spectroscopy with minimal H_2O saturation, *J. Magn. Reson. A* **109,** 129–133, (1994).

41. A. C. Wang and A. Bax, Minimizing the effects of radio-frequency heating in multidimensional NMR experiments. *J. Biomol. NMR* **3,** 715–720 (1993).

42. P. Andersson, A. Annila, and G. Otting, An α/β-HSQC-α/β experiment for spin-state selective editing of IS cross peaks, *J. Magn. Reson.* **133,** 364–367 (1998).

43. F. Cordier, A. J. Dingley, and S. Grzesiek, A doublet-separated sensitivity-enhanced HSQC for the determination of scalar and dipolar one-bond J-couplings *J. Biomol. NMR* **13,** 175–180 (1999).

44. M. Piotto, V. Saudek, and V. Sklenar, Gradient-tailored excitation for single quantum NMR spectroscopy of aqueous solutions, *J. Biomol. NMR* **2,** 661–665 (1992).

45. L. E. Kay, P. Keifer, and T. Saarinen, Pure absorption gradient enhanced heteronuclear single quantum correlation spectroscopy with improved sensitivity, *J. Am. Chem. Soc.* **114,** 10663–10665 (1992).

46. M. Ottiger and A. Bax, Determination of relative N–H^{N}, N–C′, C$^{\alpha}$–C′ and C$^{\alpha}$–H$^{\alpha}$ effective bond lengths in a protein by NMR in a dilute liquid crystalline phase, *J. Am. Chem. Soc.* **120,** 12334–12341 (1998).

47. M. Ottiger, F. Delaglio, and A. Bax, Measurement of *J* and dipolar couplings from simplified two-dimensional NMR spectra, *J. Magn. Reson.* **131,** 373–378 (1998).

48. S. Grzesiek and A. Bax, Amino acid type determination in the sequential assignment procedure of uniformly ^{13}C/^{15}N enriched proteins, *J. Biomol. NMR* **3,** 185–204 (1993).

49. A. Meissner, O. J. Duus, and O. W. Sørensen, Integration of spin-state-selective excitation into 2D NMR correlation experiments with heteronuclear ZQ/2Q π rotations for $^{1}J_{XH}$-resolved E.COSY-type measurement of heteronuclear coupling constants in proteins, *J. Biomol. NMR* **10,** 89–94 (1997).

50. A. Bax, M. Ikura, L. E. Kay, D. A. Torchia, and R. Tschudin, Comparison of different modes of two-dimensional reverse correlation NMR for the study of proteins, *J. Magn. Reson.* **86,** 304–318 (1990).

51. T. K. Mal, S. J. Matthews, H. Kovacs, I. D. Campbell, and J. Boyd, Some NMR experiments and a structure determination employing {^{15}N, ^{2}H} enriched protein, *J. Biomol. NMR* **12,** 259–276 (1998).

52. Y.-X. Wang, J. Jacob, F. Cordier, P. Wingfield, S. J. Stahl, S. Lee-Huang, D. A. Torchia, S. Grzesiek, and A. Bax, Measurement of $^{3h}J_{NC'}$ connectivities across hydrogen bonds in a 30 kDa protein, *J. Biomol. NMR* **14,** 181–184 (1999).

53. Y.-X. Wang, J. L. Marquardt, P. Wingfield, S. J. Stahl, S. Lee-Huang, D. Torchia, and A Bax, Simultaneous measurement of ^{1}H–^{15}N, ^{1}H–^{13}C′ and ^{15}N–^{13}C′ dipolar couplings in a perdeuterated 30 kDa protein dissolved in a dilute liquid crystalline phase, *J. Am. Chem. Soc.* **120,** 7385–7386 (1998).

54. R. Ishima, P. T. Wingfield, S. J. Stahl, J. D. Kaufman, and D. A. Torchia, Using amide ^{1}H and ^{15}N relaxation to detect millisecond time scale motions in perdeuterated proteins. Application to HIV-1 protease, *J. Am. Chem. Soc.* **120,** 10534–10542 (1998).

55. N. Tjandra and A. Bax, Solution NMR measurement of amide proton chemical shift anisotropy in ^{15}N–enriched proteins. Correlation with hydrogen bond length, *J. Am. Chem. Soc.* **119,** 8076–8082 (1997).

56. M. Tessari, H. Vis, R. Boelens, R. Kaptein, and G. W. Vuister, Quantitative measurement of relaxation interference effects between ^{1}H^{N} CSA and ^{1}H–^{15}N dipolar interaction: Correlation with secondary structure, *J. Am. Chem. Soc.* **119,** 8985–8990 (1997).

57. D. I. Liao, E. Silverton, Y. J. Seok, B. R. Lee, A. Peterkofsky, and D. R. Davies, The first step in sugar transport: Crystal structure of the amino-terminal domain of enzyme I of the *Escherichia coli* PEP: Sugar phosphotransferase system and a model of the phosphotransfer complex with HPr, *Structure* **4,** 861–872 (1996).

58. D. Yang and L. E. Kay, Improved line shape and sensitivity in the HNCO-family of triple resonance experiments, *J. Biomol. NMR* **14,** 273–276 (1999).

59. D. S. Garrett, R. Powers, A. M. Gronenborn, and G. M. Clore, A common sense approach to peak picking of 2D, 3D, and 4D spectra using automatic analysis of contour diagrams, *J. Magn. Reson.* **95,** 214–220 (1991).